

Anisotropy of the coherence length from critical currents in the stoichiometric superconductor LiFeAs

M. Kończykowski,¹ C. J. van der Beek,¹ M. A. Tanatar,² V. Mosser,³ Yoo Jang Song,⁴ Yong Seung Kwon,⁴ and R. Prozorov^{2,5}

¹*Laboratoire des Solides Irradiés, CNRS-UMR 7642 & CEA-DSM-IRAMIS, Ecole Polytechnique, F 91128 Palaiseau cedex, France*

²*The Ames Laboratory, Ames, IA 50011, U.S.A.*

³*ITRON/Issy Technology Center, 52 rue Camille Desmoulins, F-92130 Issy-les-Moulineaux, France*

⁴*Department of Physics, Sungkyunkwan University, Suwon, Gyeonggi-Do 440-746, Republic of Korea*

⁵*Department of Physics & Astronomy, Iowa State University, Ames, IA 50011, U.S.A.*

(Dated: 30 September 2011)

Miniature Hall-probe arrays were used to measure the critical current densities for the three main directions of vortex motion in the stoichiometric LiFeAs superconductor. These correspond to vortex lines along the c -axis moving parallel to the ab -plane, and to vortex lines in the ab -plane moving perpendicular to, and within the plane, respectively. The measurements were carried out in the low-field regime of strong vortex pinning, in which the critical current anisotropy is solely determined by the coherence length anisotropy parameter, ε_ξ . This allows for the extraction of ε_ξ at magnetic fields far below the upper critical field B_{c2} . We find that increasing the magnetic field decreases the anisotropy of the coherence length.

The determination of the electronic anisotropy in the superconducting state is a fundamental problem in multi-band type-II superconductors, that has attracted much in interest with the discovery of the iron-based materials.¹ In single band materials with an ellipsoidal Fermi surface, one can describe the anisotropy using the ratio $\varepsilon \equiv (m/M)^{1/2} < 1$ of the electron effective masses, provided that transport along the anisotropy (c -) axis of the material is coherent.² This, however, yields an oversimplified picture in which the anisotropy is temperature-independent. In multi-band superconductors, the contribution of electronic bands with different, k -dependent Fermi velocities and gap values leads to different ratios $\varepsilon_\lambda(T) = \lambda_{ab}/\lambda_c$ and $\varepsilon_\xi(T) = \xi_c/\xi_{ab}$ of the in-plane and c -axis London penetration depths $\lambda_{ab,c}(T)$ and coherence lengths $\xi_{ab,c}(T)$. The low temperature value of the penetration depth anisotropy $\varepsilon_\lambda(0) = \varepsilon(v_{F,c}/v_{F,ab})$ is determined by the anisotropy of the Fermi velocity, while its temperature dependence reflects the relative probabilities of quasi-particle excitation in the two directions. On the other hand, the coherence length anisotropy $\varepsilon_\xi \sim (v_{F,c}/v_{F,ab})(\Delta_c/\Delta_{ab})$ directly depends on the anisotropy of the superconducting gap Δ . As a result of the changing weight of superconductivity on different Fermi surface sheets and that of intra- and inter-band scattering, both ε_ξ and ε_λ are temperature^{3,4} and field-dependent,⁵ behavior exemplified by MgB₂,⁵⁻⁷ the iron-based superconductors,⁸⁻¹³ and, possibly, NbSe₂.¹⁴

Experimentally, the anisotropy parameter ε_ξ is usually determined from the ratio of the c -axis and ab -plane upper critical fields, $B_{c2}^{\parallel c} = \Phi_0/2\pi\xi_{ab}^2$ and $B_{c2}^{\parallel ab} = \Phi_0/2\pi\xi_{ab}\xi_c$,⁹⁻¹¹ while the ratio of the lower critical fields $B_{c1}^{\parallel c} = (\Phi_0/4\pi\mu_0\lambda_{ab}^2)\ln\kappa_{ab}$ and $B_{c1}^{\parallel ab} = (\Phi_0/4\pi\mu_0\lambda_{ab}\lambda_c)\ln\kappa_c$ is used to evaluate ε_λ .^{8,12} Here, $\Phi_0 = h/2e$ is the flux quantum, $\kappa_{ab} = \lambda_{ab}/\xi_{ab}$ and $\kappa_c = (\lambda_{ab}\lambda_c/\xi_{ab}\xi_c)^{1/2}$. Another approach is the direct

measurement of λ using differently oriented ac fields.¹³ Hence, ε_λ is usually obtained from measurements at low reduced fields B/B_{c2} , while ε_ξ is extracted from data in the high field regime close to B_{c2} .

Below, we show that ε_ξ at low fields can be accessed by direct measurements of the critical current density along three principal directions: j_{ab}^c for vortex lines along the c -axis moving parallel to the ab -plane, j_{ab}^{ab} for vortices parallel to the ab -plane and moving parallel to the c -axis, and j_c^{ab} for vortices again parallel to the ab -plane, but moving within the plane. Experimentally, this is not a trivial task, as the signal from usual bulk magnetometry for $\mathbf{B} \parallel ab$ will always involve contributions from both j_{ab}^{ab} and j_c^{ab} . In Fe-based superconductors, the only work that we are aware of uses transport measurements of the three critical currents in mesoscopic bridges fashioned by focused-ion beam (FIB) lithography in Sm-1111 single crystals.¹⁵ In what follows, we report on *contactless* measurements using miniature Hall-probe arrays, with the same single crystal positioned in different orientations, which allow one to unambiguously measure the critical current density for the three different situations.

In order to analyze the critical current density, we have rederived known expressions for the respective cases of weak-² and strong^{16,17} vortex pinning, for the three relevant magnetic field and current orientations. In doing so, we keep track of $\lambda_{ab,c}(T)$ and $\xi_{ab,c}(T)$ as they appear, combining them into the ratios ε_λ and ε_ξ only as a final step.¹⁸ It turns out that in the regime of strong pinning by extrinsic nm-scale defects, the anisotropy j_{ab}^{ab}/j_c^{ab} directly yields ε_ξ . In iron-based superconductors, this pinning mechanism is relevant at low magnetic fields.^{19,20} At intermediate fields, weak pinning due to scattering by dopant atoms dominates the critical current.^{19,20} Then ε_ξ is the main (but not the only) contribution to j_{ab}^{ab}/j_c^{ab} . In order to obtain unambiguous results, one should thus make sure that the critical current is measured in the

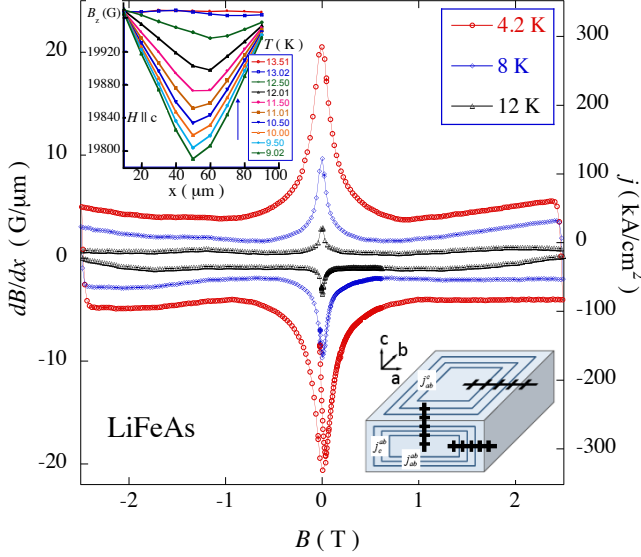


FIG. 1. (Color online) Lower inset: Experimental scheme, with the three positions of the Hall array (shown as a thick black line with intersecting segments) used to probe the j_c for the three possible orientations, as described in the text. Upper inset: Successive profiles of the magnetic induction, obtained on warming after initial zero-field cooling and the application of an external field, $\mu_0 H_a = 2 \text{ T} \parallel c$. This configuration probes j_{ab}^c . Main panel: Hysteresis loops of the in-plane local gradient dB/dx for $\mu_0 H_a \parallel c$.

limit of strong pinning. Thus, we have chosen a superconducting system with reduced intrinsic scattering, in the guise of the (tetragonal) stoichiometric compound LiFeAs.²¹ Angle-resolved photoemission²², London penetration depth²³ and first critical field measurements¹² have shown that this is a fully gapped two-band superconductor with moderate anisotropy. One of the cylindrical hole surfaces centered on the Γ -point has the smaller gap value of $\Delta = 1.5 \text{ meV}$, while the gap on the more dispersive electron surface around the M -point has $\Delta = 2.5 \text{ meV}$.²² Measurements of the anisotropic upper critical field shows that H_{c2} is of mostly orbital character for $H \parallel c$ -axis, and Pauli limited for $H \perp c$;^{9–11} there is evidence for the Fulde-Ferrell-Larkin-Ovchinnikov state for the latter configuration.⁹ A second peak effect (SPE) or “fish-tail” was reported from magnetization measurements.²⁴ For $H \parallel c$, the critical current densities range from ~ 1 ²⁵ to $\sim 100 \text{ kA/cm}^2$.²⁴ This might be indicative of different defect structures in crystals obtained in different growth procedures. Measurements of the Campbell length on our crystals have shown an even higher “theoretical” critical current density of $1 \times 10^3 \text{ kA/cm}^2$.²⁶

Single crystals of LiFeAs were grown in a sealed tungsten crucible using the Bridgman method^{12,25} and were transported in sealed ampoules. Immediately after opening, a $0.16 \times 0.19 \times 0.480 \text{ mm}^3$ rectangular parallelepiped sample was cut with a wire saw, washed and protected in mineral oil. Crystals from the same batch were

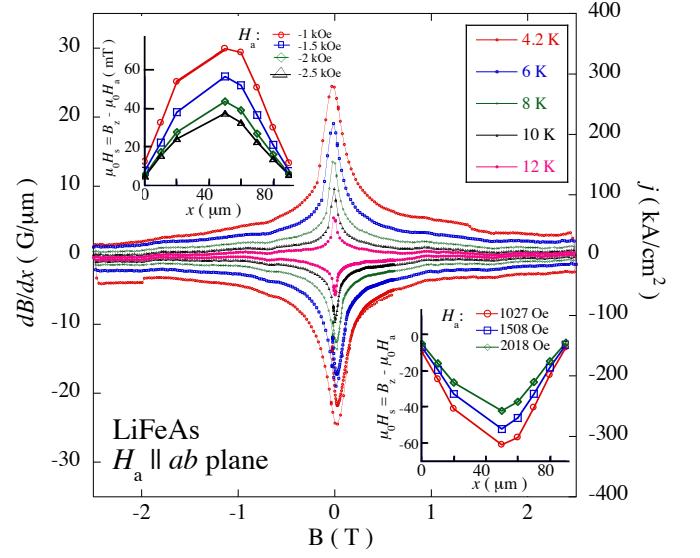


FIG. 2. (Color online) Main panel: Hysteresis loops of $dB/dx \parallel ab$, for $\mathbf{B} \parallel ab$, after zero field-cooling, measured at 4.2, 6, 8, 10, and 12 K. The right-hand ordinate shows the value of the corresponding current density j_{ab}^c . Upper inset: Profiles of the sample “self-field” $B - \mu_0 H_a$ on the decreasing field branch (third quadrant), at various H_a -values. Lower inset: Profiles of the “self-field” on the increasing field branch (first quadrant), at various H_a -values.

used for transport as well as AC and DC magnetization measurements. Overall, samples from three different batches were measured, yielding consistent results. The Hall probe arrays were tailored in a pseudomorphic AlGaAs/InGaAs/GaAs heterostructure using proton implantation. The 10 Hall sensors of the array, spaced by either 10 or $20 \mu\text{m}$, had an active area of $3 \times 3 \mu\text{m}^2$, while an 11th sensor located far from the others was used for the measurement of the applied field. The LiFeAs crystal was positioned appropriately for the measurement of the critical current density in each of the different orientations, as illustrated in the inset to Fig. 1. For the measurement of j_{ab}^c , the crystal was centered with its ab -face on the sensor array, with the array perpendicular to the long edge. For the measurement of j_{ab}^c and j_{ab}^a , the crystal was centered with its ac -face on the array, with the array perpendicular to c and to ab , respectively. In all configurations, the local magnetic induction B perpendicular to the Hall sensors (and to the sample surface) was measured along a line across the sample face, in fields up to 2.5 T .

The top inset in Fig. 1 shows typical profiles of B measured after cooling in zero magnetic field (ZFC), application of a external field $\mu_0 H_a = 2 \text{ T} \parallel c$, and warming. The straight-line profiles are quite regular and conform to the Bean model,^{27,28} which implies a homogeneous critical current density that is practically field-independent over the range of B -values in the crystal. To obtain the local screening current, we plot the spatial gradient

dB/dx versus B . The main panel in Fig. 1 shows representative hysteresis loops of dB/dx measured at 4.2, 8 and 12 K. The right ordinate shows the value of the corresponding current density $j_{ab}^c = (2/\mu_0)dB/dx$. The factor 2 corresponds to the case when B is measured on the end surface of a semi-infinite superconducting slab; a more precise evaluation can be done using the results of Brandt.²⁹ The j_{ab}^c -values, of the order of 100 kA/cm², are similar to those obtained from global measurements in the same configuration.²⁴ Because of flux creep, the measured current densities are slightly reduced with respect to the “true” critical current density, by a multiplicative factor determined by the effective experimental time scale (here, about 3 s).³⁰ The creep rate is rather modest;²⁴ in our experiment, it amounts to 2-4 % per decade of time, and is similar for j_{ab}^{ab} and j_c^{ab} , so that the ratio j_{ab}^{ab}/j_c^{ab} we shall be interested in is not appreciably altered.

The shape of the dB/dx -hysteresis loop is very similar to that obtained for other iron-based superconductors.^{19,20} It is characterized by a sharp maximum of the critical current density for $|B| \lesssim 6$ kG, behavior characteristic of a dominant contribution from strong pinning^{16,17} by nm-sized inhomogeneities.³¹ The constant dB/dx at higher fields comes from a weak “collective” pinning contribution² due to scattering of quasiparticles in the vortex cores by atomic-scale point defects.^{19,20} Figure 2 shows similar results for $H_a \parallel ab$ -plane and the Hall array $\perp c$, the configuration that probes j_c^{ab} . Again, the flux density profiles are very well described by the Bean model, although in this field orientation, the critical current density is dominated by the strong pinning contribution over the whole field range. Due to the elongated slab geometry, the configuration with $H_a \parallel ab$ does not involve a demagnetization correction, so that the relation $j_{ab} = (2/\mu_0)dB/dx$ is practically exact. With j_c^{ab} and j_{ab}^{ab} both measured in this orientation, geometry-related corrections play no role in the determination of j_{ab}^{ab}/j_c^{ab} .

The critical currents for the three directions are summarized in Fig. 3, for an applied field of 1 T. Clearly, j_{ab}^{ab} involving vortex motion along the c -axis (with vortices crossing the Fe-As planes) exceeds the other two critical currents. As expected, j_c^{ab} for easy vortex sliding along the ab -plane is the smallest. The critical current j_{ab}^c goes to zero at a lower temperature, reflecting the anisotropy of the irreversibility line in this material.

The critical current ratio j_{ab}^{ab}/j_c^{ab} for $\mathbf{B} \parallel ab$ is plotted in Fig. 4 for different values of the applied field. To analyze it, we first consider theoretical results derived for the case of weak collective pinning.² More specifically, in the regime of field-independent “single-vortex” pinning, the softer tilt- and shear moduli for vortex motion within the ab -plane imply that $j_c^{ab} = \varepsilon j_{ab}^{ab}$.² This expression that does not take into account possible differences between ε_λ and ε_ξ . A rederivation that keeps of the different contributions to the anisotropy yields $j_c^{ab} = (\varepsilon_\lambda^{5/3}/\varepsilon_\xi^{2/3})j_{ab}^{ab}$

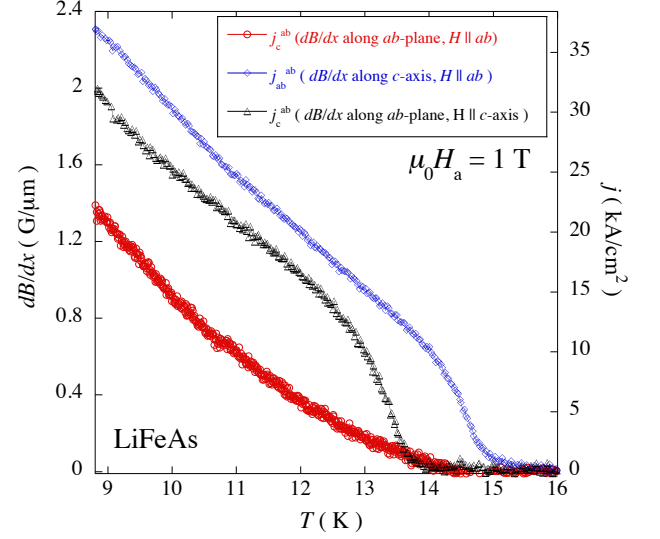


FIG. 3. (Color online) Local gradient of the magnetic induction measured in the three different configurations as function of temperature, for an applied field $\mu_0 H_a = 1$ T: (\circ) dB/dx along ab with $\mathbf{B} \parallel ab$, i.e., j_c^{ab} ; (\diamond) dB/dx along c with $\mathbf{B} \parallel ab$, i.e., j_{ab}^{ab} ; (\triangle) dB/dx along c with $\mathbf{B} \parallel c$, i.e., j_{ab}^c .

and $j_{ab}^{ab} = (\varepsilon_\lambda/\varepsilon_\xi)^{7/3}j_{ab}^c$. Hence, the anisotropy ratio

$$j_{ab}^{ab}/j_c^{ab} = \varepsilon_\lambda^{2/3}/\varepsilon_\xi^{5/3} \quad (1)$$

is mainly determined by the coherence length anisotropy.

In the present situation though, the strong pinning contribution dominates the critical current density. Then, the critical current density is determined by the direct sum of the elementary force f_p that individual inhomogeneities exert on the vortex lines.^{16,17} It is given by the expression $j_c = (f_p/\Phi_0)n_p u_0^2$,¹⁷ where n_p is the defect density, and Φ_0 is the flux quantum. The trapping radius u_0 is the largest distance, perpendicular to the field direction, on which a pin can be effective. The critical current anisotropy is thus determined by the anisotropy of f_p , and that of u_0 . The former is determined by the anisotropy of λ and ξ , and by the geometric anisotropy of the pins, $\varepsilon_b = \ln(1 + b_{ab}^2/2\xi_{ab}^2)/\ln(1 + b_{ab}b_c/2\varepsilon_\xi\xi_{ab}^2) < 1$. Here, b_{ab} and b_c are the mean extent of the pins in the ab and c -direction, respectively. At low fields, the u_0 -anisotropy is determined only that of the vortex line tension, and is therefore field-independent. We find that $j_c^{ab} = \varepsilon_\lambda^2 \varepsilon_b^{-3/2} j_s^c$, while $j_{ab}^{ab} = (\varepsilon_\lambda^2/\varepsilon_b^{3/2} \varepsilon_\xi) j_s^c$. At higher fields, u_0 is determined by the intervortex interaction, leading to the ubiquitous decrease of the critical current density as $B^{-1/2}$. Then, $j_c^{ab} = \varepsilon_b^{-2} \varepsilon_\lambda j_s^c$, while $j_{ab}^{ab} = (\varepsilon_\lambda/\varepsilon_b^2 \varepsilon_\xi) j_s^c$. In both cases,

$$j_{ab}^{ab}/j_c^{ab} = 1/\varepsilon_\xi. \quad (2)$$

Thus, the experimental ratio j_{ab}^{ab}/j_c^{ab} , plotted in Fig. 4, directly measures the coherence length anisotropy.

In spite of the fact that we could only evaluate the anisotropy above $T = 9$ K, it is clear that the extrapo-

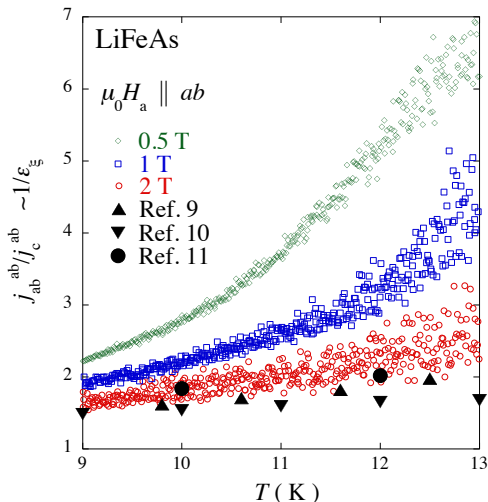


FIG. 4. (Color online) Critical current ratio $j_{ab}^{ab}/j_c^{ab} \sim 1/\varepsilon_\xi$ for applied magnetic fields of (\diamond) 0.5 T; (\square) 1 T; (\circ) 2 T.

lated values of $1/\varepsilon_\xi$ at low temperature are of the order 1.5 – 2. The anisotropy ($\sim 1/\varepsilon_\xi$) increases with increasing temperature to become as large as 6–7 at $T = 13$ K, an experimental upper limit imposed by the increasing role of flux creep at higher T . The anisotropy becomes smaller and less T -dependent at higher magnetic field, and merges with the results obtained from the B_{c2} -ratios reported in Refs. 9–11 for a field as low as 2 T. Both the magnitude and the T -dependence of ε_ξ are reminiscent of that of ε_λ obtained on the 1111 family of iron-based superconductors.⁸ Notably, ε_ξ is strongly temperature dependent at low fields, and less so at higher magnetic fields.

Since the Fermi velocity is unaffected by field, a plausible framework for our observations is the temperature-³² and field-dependent relative contribution of the two superconducting gaps to the effective superconducting coherence length. In particular, the evolution of ε_ξ suggests that the relative weight of the gap on the more two-dimensional hole surface progressively decreases as the magnetic field is increased. For fields higher than 2 T, the gap on the three-dimensional electron surface would determine all superconducting properties related to the coherence length. This is consistent with recent thermal conductivity measurements that suggest that at fields as low as $0.1B_{c2}(0)$ (*i.e.* 2 T), LiFeAs behaves as a single band superconductor. In that limit, the anisotropy of the coherence length and of the penetration depth are expected to be similar, and rather temperature independent. This is indeed the trend observed in the measurements: the high-field coherence length anisotropy seem

to behave very similarly to reported results for the penetration depth anisotropy.³⁴ It is to be noted that as the magnetic field is increased, the vortex core radius should plausibly shrink, such as this occurs in NbSe₂.¹⁴ Also, the core structure should be modified.³² This does not affect the ratio of the coherence lengths discussed here.

The field-dependence of ε_ξ may explain why the weak collective pinning contribution to the critical current density is more important for fields oriented parallel to c . The values of ε_ξ and ε_λ are very similar at fields above 1 – 2 T at which this contribution manifests itself. Hence, the weak pinning part of the critical current should be nearly the same for the two field orientations, as in a single band superconductor. At lower fields, it should be enhanced for $H \parallel ab$, but this is not perceptible because it remains masked by the strong pinning contribution. On the other hand, strong pinning is enhanced for all values of $H \parallel ab$ because its dependence on ε_ξ through ε_b .

In conclusion, we present a direct technique for the measurement of the critical current anisotropy in uniaxial type II superconductors. The technique crucially relies on the use of a local probe of the magnetic induction, in this case, miniature Hall probe arrays. In the situation of strong pinning by extrinsic extended point defects, the ratio of the critical current densities along the ab -plane and the c -axis, for field oriented along the ab -plane, directly yields the coherence length anisotropy. We apply the method to infer the coherence length anisotropy $1/\varepsilon_\xi$ of LiFeAs at much lower magnetic fields than commonly reported. We interpret the results in terms of the gap anisotropy, and find that this is reduced to its value near B_{c2} by the application of a magnetic field as low as 2 T.

ACKNOWLEDGMENTS

We thank V.G. Kogan for useful discussions and Dr. S. Bansropun and his group at Thales-TRT, Palaiseau for the careful processing of the Hall sensors. This work was supported by the French National Research agency, under grant ANR-07-Blan-0368 “Micromag”. The work at The Ames Laboratory was supported by the U.S. Department of Energy, Office of Basic Energy Sciences, Division of Materials Sciences and Engineering under contract No. DE-AC02-07CH11358. Work at SKKU was partially supported by Basic Science Research Program through the National Research Foundation of Korea (NRF) funded by the Ministry of Education, Science and Technology (2010-0007487). The work of R. Prozorov in Palaiseau was funded by the St. Gobain Chair of the Ecole Polytechnique.

¹ D. C. Johnston, Advances in Physics **59**, 803–1061 (2010).

² G. Blatter, M.V. Feigel'man, V.B. Geshkenbein, A.I.

Larkin, and V.M. Vinokur, Rev. Mod. Phys. **66**, 1125 (1994).

- ³ A. Gurevich, *Physica C* **456**, 160 (2007).
- ⁴ V. G. Kogan, *Phys. Rev. B* **66**, 020509 (2002).
- ⁵ T. Nojima, H. Nagano, A. Ochiai, H. Aoki, B. Kang, and S.-I. Lee, *Physica C* **445-448**, 42 (2006).
- ⁶ Z. X. Shi, M. Tokunaga, T. Tamegai, Y. Takano, K. Togano, H. Kito, and H. Ihara, *Phys. Rev. B* **68**, 104513 (2003).
- ⁷ J. D. Fletcher, A. Carrington, O. J. Taylor, S. M. Kazakov, and J. Karpinski, *Phys. Rev. Lett.* **95**, 097005 (2005).
- ⁸ R. Okazaki, M. Konczykowski, C. J. van der Beek, T. Kato, K. Hashimoto, M. Shimosawa, H. Shishido, M. Yamashita, M. Ishikado, H. Kito, A. Iyo, H. Eisaki, S. Shamoto, T. Shibauchi, and Y. Matsuda, *Phys. Rev. B* **79**, 064520 (2009).
- ⁹ K. Cho, H. Kim, M. A. Tanatar, Y. J. Song, Y. S. Kwon, W. A. Coniglio, C. C. Agosta, A. Gurevich, and R. Prozorov, *Phys. Rev. B* **83**, 060502 (2011).
- ¹⁰ N. Kurita, K. Kitagawa, K. Matsubayashi, A. Kismarhardja, Eun-Sang Cho, J. S. Brooks, Y. Uwatoko, S. Uji, and T. Terashima, *J. Phys. Soc. Japan* **80**, 013706 (2011).
- ¹¹ Seunghyun Khim, Bumsung Lee, Jae Wook Kim, Eun Sang Choi, G. R. Stewart, and Kee Hoon Kim, *Phys. Rev. B* **84**, 104502 (2011).
- ¹² Yoo Jang Song, Jin Soo Ghim, Jae Hyun Yoon, Kyu Joon Lee, Myung Hwa Jung, Hyo-Seok Ji, Ji Hoon Shim, Yunkyu Bang, and Yong Seung Kwo, *Europhys. Lett.* **94**, 57008 (2011).
- ¹³ R. Prozorov and V. G. Kogan, *Rep. Prog. Phys.* **74**, 124505 (2011).
- ¹⁴ F. D. Callaghan, M. Laulajainen, C. V. Kaiser, and J. E. Sonier, *Phys. Rev. Lett.* **95**, 197001 (2005).
- ¹⁵ Philip J.W. Moll, Roman Puzniak, Fedor Balakirev, Krzysztof Rogacki, Janusz Karpinski, Nikolai D. Zhigadli and Bertram Batlogg, *Nature Mat.* **9**, 628 (2010).
- ¹⁶ Yu. N. Ovchinnikov and B. I. Ivlev, *Phys. Rev. B* **43**, 8024 (1991).
- ¹⁷ C. J. van der Beek, M. Konczykowski, A. Abaloshev, I. Abalosheva, P. Gierlowski, S. J. Lewandowski, M. V. Indenbom, and S. Barbanera, *Phys. Rev. B* **66**, 024523 (2002).
- ¹⁸ C.J. van der Beek, M. Konczykowski, and R. Prozorov, to be published.
- ¹⁹ Cornelis J. van der Beek, Marcin Konczykowski, Shigeru Kasahara, Takahito Terashima, Ryuji Okazaki, Takasada Shibauchi, and Yuji Matsuda, *Phys. Rev. Lett.* **105**, 267002 (2010).
- ²⁰ C. J. van der Beek, G. Rizza, M. Konczykowski, P. Fertey, I. Monnet, Thierry Klein, R. Okazaki, M. Ishikado, H. Kito, A. Iyo, H. Eisaki, S. Shamoto, M. E. Tillman, S. L. Budko, P. C. Canfield, T. Shibauchi, and Y. Matsuda, *Phys. Rev. B* **81**, 174517 (2010).
- ²¹ X. C. Wang, Q. Q. Liu, Y. X. Lv, W. B. Gao, L. X. Yang, R. C. Yu, F. Y. Li, and C. Q. Jin, *Solid State Comm.* **148**, 538 (2008).
- ²² S. V. Borisenko, V. B. Zabolotnyy, D. V. Evtushinsky, T. K. Kim, I. V. Morozov, A. N. Yaresko, A. A. Kordyuk, G. Behr, A. Vasiliev, R. Follath, and B. Büchner *Phys. Rev. Lett.* **105**, 067002 (2010).
- ²³ H. Kim, M. A. Tanatar, Yoo Jang Song, Yong Seung Kwon, and R. Prozorov, *Phys. Rev. B* **83**, 100502 (2011).
- ²⁴ A. K. Pramanik, L. Harnagea, C. Nackle, A. U. B. Wolter, S. Wurmehl, V. Kataev, and B. Büchner, *Phys. Rev. B* **83**, 094502 (2011).
- ²⁵ Yoo Jang Song, Jin Soo Ghim, Byeong Hun Min, Yong Seung Kwon, Myung Hwa Jung, and Jong-Soo Rhyee, *Appl. Phys. Lett.* **96**, 212508 (2010).
- ²⁶ Plengchart Prommapan, Makariy A. Tanatar, Bumsung Lee, Seunghyun Khim, Kee Hoon Kim, and Ruslan Prozorov, *Phys. Rev. B* **84**, 060509 (2011).
- ²⁷ C.P. Bean, *Phys. Rev. Lett.* **8**, 6 (1962).
- ²⁸ E. Zeldov, J. R. Clem, M. McElfresh and M. Darwin, *Phys. Rev. B* **49**, 9802 (1994).
- ²⁹ E. H. Brandt, *Phys. Rev. B* **58**, 6506 (1998).
- ³⁰ C. J. van der Beek, G.J. Nieuwenhuys, P.H. Kes, H.G. Schnack, and R. Griessen *Physica C* **197**, 320 (1992).
- ³¹ S. Demirdiř, C. J. van der Beek, Y. Fasano, N. R. Cejas Bolecek, H. Pastoriza, D. Colson, and F. Rullier-Albenque, *Phys. Rev. B* **84**, 094517 (2011).
- ³² L. Komendová, M. V. Milořević, A. A. Shanenko, and F. M. Peeters, *Phys. Rev. B* **84**, 064522 (2011).
- ³³ M. A. Tanatar, J.-Ph. Reid, S. René de Cotret, N. Doiron-Leyraud, F. Laliberté, E. Hassinger, J. Chang, H. Kim, K. Cho, Yoo Jang Song, Yong Seung Kwon, R. Prozorov, and Louis Taillefer, *Phys. Rev. B* **84**, 054507 (2011).
- ³⁴ K. Sasmal, Z. Tang, F. Y. Wei, A. M. Guloy, and C.W. Chu, *Phys. Rev. B* **81**, 144512 (2010).